

1 **Climatic characteristics of the Jianghuai cyclone and its linkage with**
2 **precipitation during the Meiyu period from 1961 to 2020**

3 Ran Zhu¹, Lei Chen^{1,2}

4 ¹Department of Atmospheric Science, School of Environmental Studies, China University of
5 Geosciences, Wuhan, 430074, China

6 ²Centre for Severe Weather and Climate and Hydro-Geological Hazards, Wuhan, 430074, China

7 Correspondence to: Lei Chen (leichen@cug.edu.cn)

8 **Abstract.** This study examines the climatic characteristics of 202 Jianghuai cyclones
9 and their linkage with precipitation during the Meiyu period from 1961 to 2020. The
10 results show that cyclones mainly originate from eastern Hubei Province and south-
11 central Anhui Province, and further explored the statistical characteristics of the
12 strength, radius, and their positive correlation. When studying the interdecadal variation
13 of cyclones, we found that there is a similar trend between the interdecadal variation of
14 cyclones and Meiyu precipitation. Therefore, we further investigate the correlation
15 between the Jianghuai cyclones and the precipitation during the Meiyu period. There is
16 a positive correlation coefficient of 0.769 between them. It's worth mentioning that the
17 percentage of precipitation affected by cyclone activities can reach up to 47%. The
18 anomalous increase in precipitation caused by cyclones above 27°N can reach a
19 maximum of 7 mm/day. When the cyclone existed, there was a significant altitude
20 anomaly of negative geopotential height can be traced to day -4 at the 500 hPa level
21 over Mongolia. The abnormally enhanced WPSH, southwest jet and negative
22 geopotential height are the dominant factors causing abnormal precipitation during
23 Jianghuai cyclones. Before and after the cyclone developed, water vapor flux and
24 divergence from low latitudes abnormally increased. These provide sufficient water
25 vapor conditions for the generation of cyclone precipitation.

1. Introduction

Meiyu is a special rainy season due to the progress of the East Asian summer monsoon. The East Asian summer monsoon broke out in the South China Sea in mid-May and then advanced northward, forming rain bands in South China, the Jianghuai region, the Korean Peninsula and Japan (Ding et al., 2004,2007; Qian et al., 2000). The name for this special rainy season is called Meiyu in China, while it is called Changma in South Korea and it is called Baiu in Japan (Ninomiya et al., 1987; Oh et al., 1997; Saito. 1995;). Meiyu front is one of the important weather systems affecting summer precipitation in the middle and lower reaches of the Yangtze River (Pang et al., 2013; Wang et al., 2014; Zhou et al., 2022; Tao et al., 1979). From mid-June to early July, the east of Yichang, Hubei Province, has continuous rains and short sunshine. These conditions are accompanied by heavy rainfall, strong wind and other weather phenomena in these areas during the Meiyu period (Ding. 1992; Zhao et al., 2021; Zhou et al., 2017). In China, the mean annual precipitation during the Meiyu period in the Jianghuai River Basin can reach 300 mm, accounting for 30%-40% of the mean annual total precipitation, and even up to 500 mm or more in the extreme Meiyu period (Liu et al., 2020). Historically, most of the summer floods disasters are caused by precipitation anomalies in the Meiyu period. Some scholars have studied and analyzed the representative floods of 1996, 1998, 2016 and 2020 (Bao et al., 2021; Su et al., 2021; Zhao et al., 2018; Zhong et al., 2023). These floods, caused by the Meiyu front, had adverse effects on people's safety, lives and property (Yan et al., 2021). Scholars in China have divided rainstorms caused by Meiyu fronts into three types (Zhang et al., 2004). The first type is the β mesoscale convective rainstorm on the Meiyu front. This type of rainstorm has a range of less than 300 km with strong intensity and a fast formation process (He et al., 2007). It is difficult to forecast before 12 hours and can be detected only by using radar to make a proximity forecast (Zhang et al., 2002). The second type is the persistent rainstorm located in front of the high-altitude low-pressure tank in the western part of the Meiyu front. It is characterized by a long duration of approximately 5 days but appears less frequently, mainly in western Hubei and western

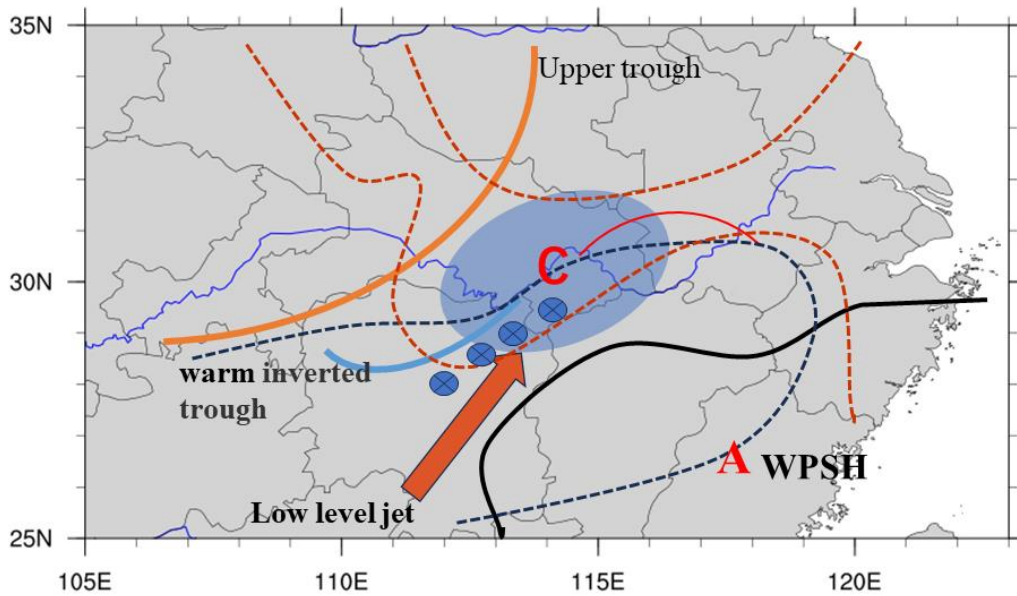
55 Hunan and Sichuan (Cai et al., 2021; Wu et al., 2020;). The last type is the rainstorm
56 caused by the Jianghuai cyclone located east of the origin of the Meiyu. The Jianghuai
57 cyclones are affected by the thermal conditions of the sea and land and likely occur in
58 the eastern part of the Meiyu front (Wang et al., 2016). The positive vorticity advection
59 in front of the high-altitude trough and the warm advection in front of the front promote
60 the eastward movement and development of the cyclone (Shen et al., 2019; Zhang et
61 al., 2016). During the development of the cyclone, the lower levels are dominated by
62 the southwest warm and humid airflow, and the high levels are mainly affected by dry
63 and cold air (Zhao et al., 2008). This type of rainstorm has a large range, high intensity
64 and long duration of precipitation (Wang et al., 2012; Xu et al., 2011).

65 Scholars' studies on Jianghuai cyclones during the Meiyu period were initially
66 based on individual case analysis. Xu et al. (2013) studied a cyclone process in 2011
67 and found that the cyclone process lasted up to 36 h. The cyclone rainstorm was
68 distributed on the south side of the cyclone. Heavy precipitation during the whole
69 cyclone mainly occurred in the lower reaches of the Yangtze River. Wu et al. (2020)
70 studied 2 different cyclone rainstorm processes. They found that rainfall is directly
71 proportional to cyclone intensity. There is a strong convergence center of water vapor
72 flux during cyclone development. Zhou et al. (2020) found that a tornado was generated
73 from the cyclone occlusion stage on July 22. The tornado was under the influence of a
74 strong and fast Jianghuai cyclone and produced heavy precipitation accompanied by
75 thunderstorm phenomena. With the improvement of cyclone identification methods and
76 reconstruction of reanalysis data, statistical studies of cyclones have been further
77 developed (Simmonds et al., 1999; 2000; Wernli et al., 2006). Yang et al. (2010)
78 modeled the rainstorm process in the lower reaches of the Yangtze River from 1998 to
79 2005. The cyclones accounted for 62.5% of the rainstorm cases, and more than 70% of
80 the cyclones could develop and produce rainstorms. The Jianghuai cyclone located in
81 the lower reaches of the Yangtze River generally exists in the lower troposphere at 700
82 hPa. The horizontal scale is within 400 km, and the life period on land is generally less
83 than 48 h. Wang et al. (2015) found that the number of cyclones was lower and their

84 intensity was weak in the 1980s and 1990s. In the early 2000s, cyclones were more
85 frequent, and their intensity increased. After 2010, there was again a decreasing trend.
86 Zhang et al. (2018) divided 60 cases of extreme precipitation in the middle reaches of
87 the Yangtze River from 2008 to 2015 into five types. Among them, the extreme
88 precipitation of the Jianghuai cyclone type accounted for 30%. The stable and
89 maintained Western Pacific subtropical high (WPSH) system is one of the important
90 reasons for the strong precipitation produced by cyclones. Because of the weak cold air
91 force, the intensity of the Jianghuai cyclone is weaker than that in spring (Zhou et al.,
92 2017). The daily analysis of the Jianghuai cyclones in the Meiyu period is easy to ignore.
93 All these studies indicate that the Jianghuai cyclone is an important weather system that
94 causes heavy rainfall during the Meiyu period in the middle and lower reaches of the
95 Yangtze River (Wu et al., 2021; Zhang et al., 2018; Zhu et al., 1998).

96 Research on the climatic characteristics and precipitation effects of Jianghuai
97 cyclones during the Meiyu period in the past 60 years has not yielded clear results. In
98 this study, the relative vorticity method is used to objectively identify and track
99 cyclones based on reanalysis data provided by ERA5. The climatological characteristics
100 of the Jianghuai cyclones during this period are studied. We analyze the correlation
101 between Jianghuai cyclone activity and precipitation. This study provides a reference
102 for the long-term and short-term forecasting of precipitation in the Meiyu period.

103 The remainder of the present paper is organized as follows. Section 2 of this paper
104 presents the dataset and analytical methods. In Section 3, we show the climatology
105 composite of the cyclone tracks, genesis locations, intensity, lifetime and so on. There
106 is a positive correlation between the frequency of cyclonic activity and precipitation in
107 the Meiyu period. The relationship between them is studied by means of the
108 geopotential height anomaly and water vapor flux anomaly. Section 4 provides the main
109 discussion and findings of this study.



110

111 Fig.1 Schematic diagram of the main weather system and the structure of temperature
 112 and pressure field in the middle and low levels of the Jianghuai cyclone. (Red dotted
 113 line: isotherm; Solid black line: contour line; Blue dot: precipitation area; Solid orange
 114 line: 500 hPa upper-level trough; Red arrow: low level jet; Black dotted line: warm
 115 inverted trough; Solid red line: warm shear; Solid blue line: cold shear; Letter C:
 116 cyclone; Letter A: WSPH.)

117 2. Data and methods

118 2.1 Data

119 The time span of all the data is 60 years from 1961 to 2020, and the study area is
 120 located at 108°E-123°E, 27°N-34°N. We use the ERA5 relative vorticity hourly data
 121 (850 hPa) released by the European Centre for Medium Range Weather Forecasts
 122 (ECMWF) for Jianghuai cyclone identification and tracking. The spatial resolution of
 123 the data is 0.25°×0.25°, and the temporal resolution is 6 h. Every 6 h was defined as a
 124 step. The data of geopotential height, wind field, and specific humidity are daily data
 125 processed from ERA5 hourly data with a spatial resolution of 0.25°×0.25° (Hersbach
 126 et al., 2018). The geopotential height and wind field data include pressure levels of
 127 approximately 500 hPa, 700 hPa and 850 hPa. The specific humidity data include

128 pressure levels of approximately 500 hPa, 700 hPa and 850 hPa. The precipitation data
129 are from the CN05.1 grid point observation dataset compiled by the National
130 Meteorological Information Center of China Meteorological Administration with a
131 resolution of $0.25^{\circ} \times 0.25^{\circ}$.

132 **2.2 Methods**

133 The objective identification and tracking method for cyclones used in this paper is
134 the vorticity tracking method proposed by Hodges (1994, 1995). The first step is to use
135 the relative vorticity field at the 850 hPa pressure level corresponding to every moment
136 of the cyclone to determine the range of each cyclone. The second step is to find the
137 feature points. In the process of finding the feature points, the extreme point and the
138 centroid point are the alternatives. Corresponding to the global relative vorticity grid
139 data of each time point, several feature points can be found, and each point represents
140 a cyclone. The third step is to match the track of each cyclone under the given time
141 span. In Hodges (1994), the assumed data used are defined on a rectangular grid, and
142 each time step is initially processed to identify the maximum or minimum value of the
143 "object" on the positioning grid. The tracking method is feasible on high-resolution
144 grids, but on low-resolution grids, the feature points may not be sufficient to produce
145 smooth trajectories, so the smoothness of the tracking algorithm is effectively limited.
146 Hodges (1995) proposed tracking feature points on the unit sphere, which would
147 become the feature point matching problem of grid data for adjacent time points in
148 cyclone tracking. If the algorithm is reasonable, there is no "discontinuity" mutation in
149 the final arriving cyclone track, and the track is more accurate.

150 In addition to the relative vorticity method of tracking proposed by Hodges,
151 different methods of cyclone identification have also been proposed by other scholars.
152 Lu (2017) improved the extratropical cyclone identification and tracking method
153 involving the nine-point pressure minimum. Jiang et al. (2020) proposed an algorithm
154 for identifying extratropical cyclones on the basis of gridded data. This algorithm is
155 named the eight-section slope detection method. Among them, the most commonly

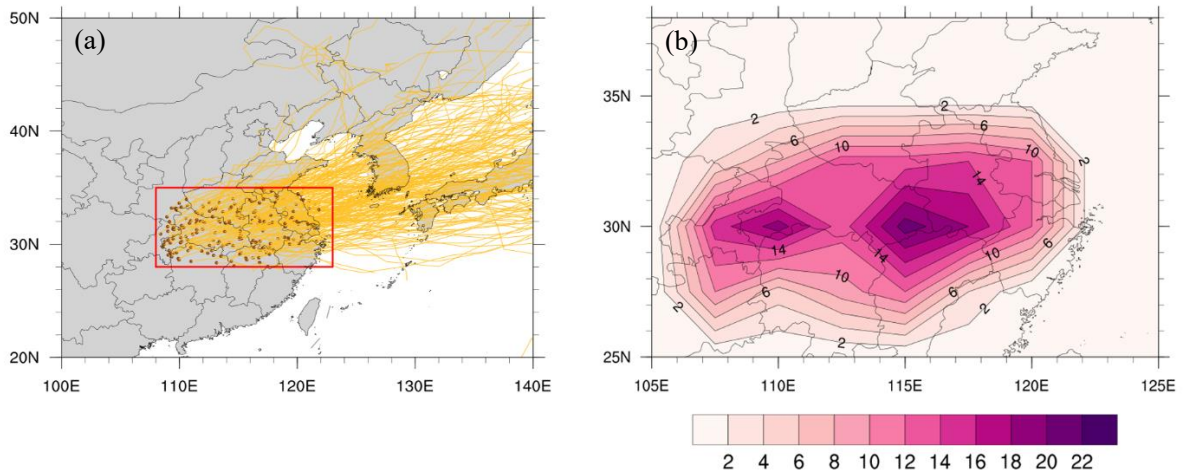
156 used cyclone tracking methods are the mean sea level pressure method (SLP) and 850
157 hPa relative vorticity method. Mailier et.al (2006) and Zhang et.al (2012) studied the
158 tracks of individual cyclones in these two methods. Both of them found 850 hPa relative
159 vorticity method can identify and detect cyclone center earlier than the SLP method
160 (Mailier et al., 2006). The reason for this result is that SLP is easily affected by
161 topography and large-scale background circulation shear vorticity (Hodges, 1994). So
162 based on this advantage of the relative vorticity method, we select the 850 hPa relative
163 vorticity tracking method. The relative vorticity tracking method can detect low vortex
164 systems earlier and track cyclones for a longer period of time with better stability. When
165 the closed pressure levels are not visible on the satellite map, the vorticity tracking
166 method can still continue to track the cyclone, improving the accuracy of cyclone track
167 data.

168 **3. Results**

169 **3.1 Climatic characteristics of the Jianghuai cyclone during the Meiyu period**

170 A total of 202 Jianghuai cyclones existed during the Meiyu period from 1961 to
171 2020. The range of cyclone genesis locations defined by the Jiangsu Meteorological
172 Administration (2017) and the characteristics of the relative vorticity tracking method
173 were used. We adjust the genesis location and remove the cyclones that are generated
174 at sea and have no effect on land precipitation (108°E - 123°E , 28°N - 35°N). Figure 2a
175 shows the distribution of Jianghuai cyclone tracks. The brown dots represent the genesis
176 locations of the first occurrence of the Jianghuai cyclone. The yellow lines indicate the
177 tracks of the cyclones. As shown in the figure, the tracks of the cyclone are mainly
178 eastward and northeast. These two kinds of tracks are related to the upper-level guide
179 airflow of 500~700 hPa (Wei et al., 2013). The northeast track is mainly due to the
180 southwest warm and moist air on the edge of the WPSH. The east track is mainly related
181 to the location of the WPSH. Figure 2b shows the frequency of cyclone occurrence
182 refers to the total number of cyclones during the Meiyu period from 1961 to 2020. The
183 genesis locations of cyclones are mainly located in the middle and lower reaches of the

184 Yangtze River and the Huaihe River basin, with an east–west band distribution (Wang
 185 et al., 2015; Wu et al., 2021). The frequency of occurrence refers to the total number of
 186 cyclones during the Meiyu period from 1961 to 2020 is higher in the region of the Hubei
 187 and Chongqing junction, eastern Hubei, northern Jiangxi, south-central Anhui, Jiangsu
 188 and Zhejiang. Research has found that the genesis locations of cyclones are closely
 189 related to the landform (Xu 2021; Zhang et al., 2012).

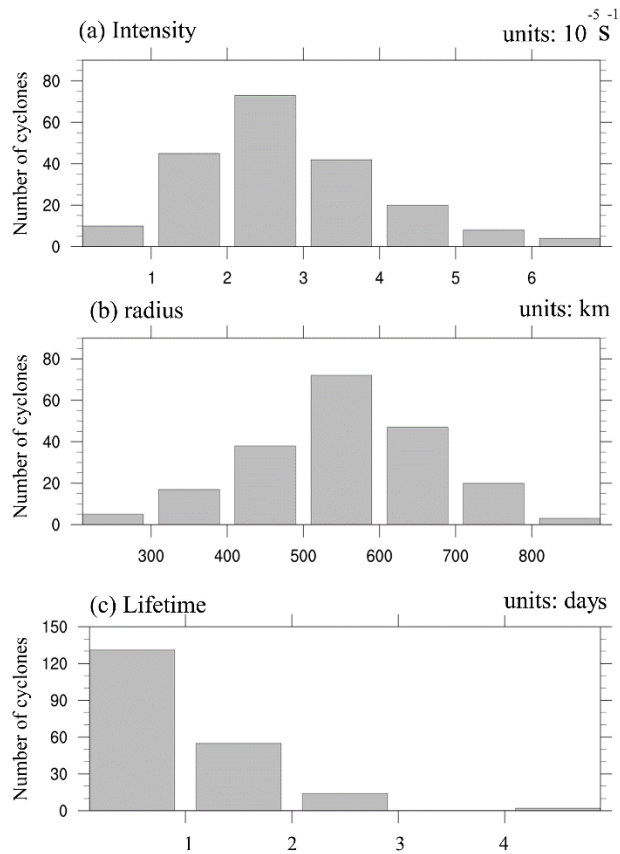


190 Fig 2. Distribution of the cyclone genesis locations, tracks (a) and the frequency of
 191 genesis locations refers to the total number of cyclones (b) during the Meiyu period
 192 from 1961 to 2020 (The brown dots represent the genesis locations. The yellow lines
 193 indicate the tracks).

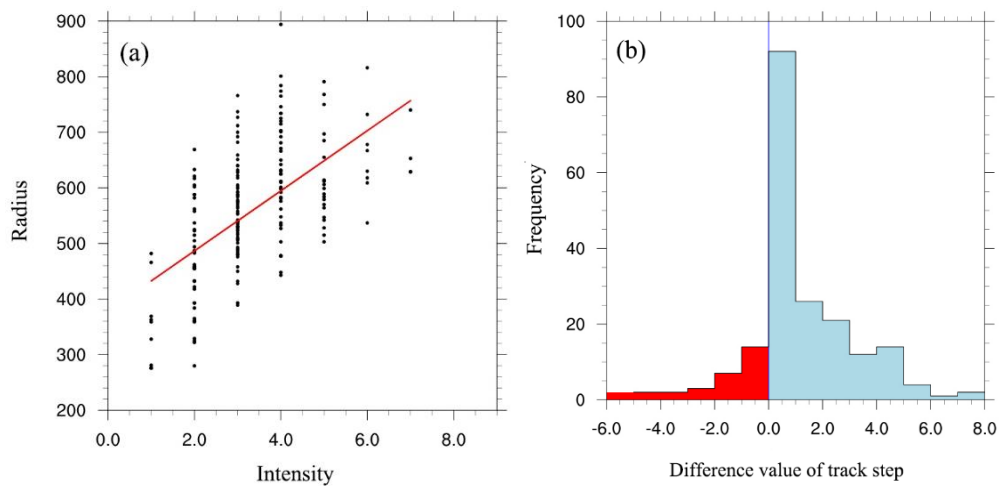
194 To examine the climatological characteristics of Jianghuai cyclones over 60 years,
 195 we focus on the intensity, radius, and lifetime of cyclones on land. The intensity of the
 196 Jianghuai cyclone is defined as the relative vorticity intensity of the 850 hPa cyclone
 197 center. The larger the relative vorticity intensity is, the stronger the cyclone intensity is.
 198 Figure 3a shows that among the 202 selected cyclones, the intensity of the cyclone
 199 center mainly ranges from $0 \times 10^{-5} \text{ s}^{-1}$ to $7 \times 10^{-5} \text{ s}^{-1}$. When the intensity of the cyclone
 200 center is less than $3 \times 10^{-5} \text{ s}^{-1}$, the number of cyclones increases with increasing intensity;
 201 when it is larger than $3 \times 10^{-5} \text{ s}^{-1}$, the number of cyclones decreases with weakening
 202 intensity. The number of cyclones in the range of $2 \times 10^{-5} \text{ s}^{-1}$ to $3 \times 10^{-5} \text{ s}^{-1}$ has the largest
 203 proportion, accounting for 36% of the total number of cyclones. A total of 180 cyclones

204 are in the range of $1 \times 10^{-5} \text{ s}^{-1}$ to $5 \times 10^{-5} \text{ s}^{-1}$ in intensity, accounting for 89%. Figure 3b
205 shows the relationship between the radius of cyclones and the number of cyclones. Most
206 of the cyclones have an average radius between 300 and 800 km, accounting for 96%
207 of the total number. The number of cyclones with radii between 500 and 600 km is the
208 largest, accounting for 35%. Figure 3c shows the relationship between the time of
209 cyclones affecting precipitation on land and the number of cyclones. Most of the
210 cyclones affect precipitation on land for 1-3 days, and only one cyclone affects
211 precipitation on land for more than 3 days. The number of cyclones that affected
212 precipitation on land within 2 days was 186, accounting for 92% of the total number.

213 The intensity of a cyclone is one of the factors affecting its precipitation and impact
214 range during the Meiyu period (Zhao et al., 2010). Figure 4a shows a positive
215 correlation between the maximum intensity and the maximum radius of cyclone
216 development. The stronger the intensity of a cyclone is, the larger its radius. Therefore,
217 the horizontal scale of most strong cyclones is larger than that of weak cyclones, the
218 precipitation is greater, and the precipitation range is larger. From the distribution of
219 difference value of track step between the maximum intensity and the radius of the
220 cyclone shown in Figure 4b, the number of cyclones that reach both at the same time
221 accounts for 45% of the total number of cyclones. Of the remaining Jianghuai cyclones,
222 more reach the maximum intensity first and continue to develop to the maximum
223 horizontal scale.

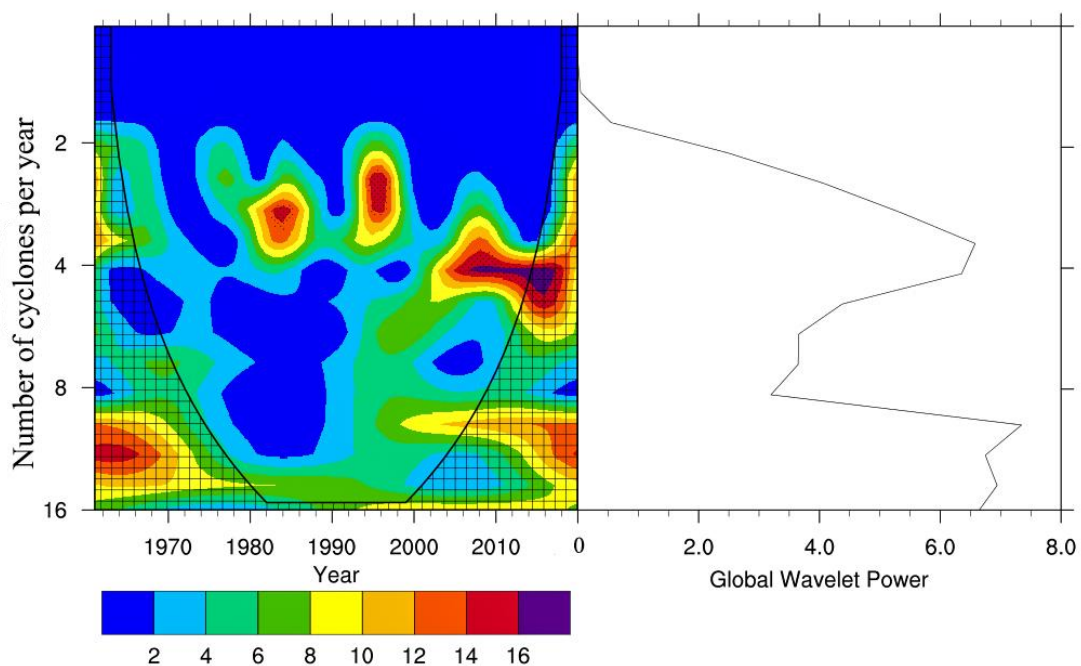


224 Fig 3. Distributions of the number of selected cyclones versus their (a) intensities (units:
 225 10^{-5} s^{-1}), (b) radii (units: km), and (c) lifetimes (units: days).



226 Fig 4. Correlation between maximum intensity (units: 10^{-5} s^{-1}) and maximum radius
 227 (units: km) (a) and their difference value of track step during the development of the
 228 Jianghuai cyclone in the Meiyu period (b).

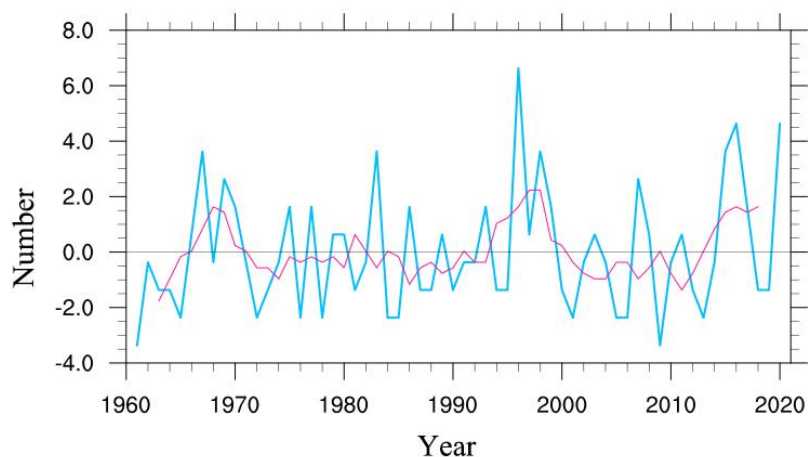
229 The frequency of Jianghuai cyclone occurrence refers to the total number of
230 cyclones is characterized by multiperiod variation (Figure 5). The shaded area in the
231 figure indicates that the 95% confidence interval according to the T test is passed.
232 Strong 2–4-year quasiperiodic variation is observed for 1980-1990 and 1990-2000.
233 After 2000, the quasiperiodic change in cyclones is approximately 4-5 years. This
234 change period corresponds to the period of abnormal change in Meiyu. Chen et al.
235 (2019) pointed out that 3~4 years of quasiperiodic change is the main component of
236 abnormal changes in Meiyu when studying the quasiperiodic change in Meiyu. This
237 quasiperiodic variation component is mainly influenced by the out-of-ocean forcing of
238 the Indian Ocean dipole (IOP), which changes from the ENSO in the previous winter
239 to late spring and early summer with seasonal changes (Liang et al., 2018). During the
240 positive phase of the IOP, the strong warming of the Indian Ocean triggers a strong
241 Indian monsoon. This leads to a strengthening of the WPSH and an increase in
242 precipitation in southern China. The southwestern rapids, which are enhanced by the
243 positive IOP, also provide sufficient water vapor and warm advection to generate
244 favorable conditions for the development of the Jianghuai cyclone.



245 Fig 5. Periodic wavelet analysis diagram of Jianghuai cyclones during the Meiyu period

246 from 1961 to 2020 (units: year) (shadow indicates passing the 95% confidence interval
247 according to the T test).

248 Jianghuai cyclones are not only characterized by multiperiod variability but also
249 have significant interdecadal variability. Figure 5 shows the activity frequency anomaly
250 and 5-year sliding average of cyclones during the Meiyu period from 1961 to 2020. The
251 frequency of cyclone activity was the highest in 1996 and the lowest in 1961 and 2009.
252 In the long term, the frequency of cyclone activity in the middle and lower reaches of
253 the Yangtze River increased in 1965-1970, in 1990-2000 and after 2010. It decreased
254 in 1970-1990 and 2000-2010. The interdecadal variability trend of Jianghuai cyclones
255 is similar to the interdecadal variability trend of precipitation during the Meiyu period
256 (Chen et al., 2019).



257 Fig 6. Frequency anomaly and 5-year sliding average of cyclones. The blue line shows
258 the anomalies in the number of cyclones, and the pink line shows the 5-year sliding
259 average of the anomalies.

260 **3.2 Linkage between cyclone activity and concurrent rainfall in the middle and** 261 **lower reaches of the Yangtze River.**

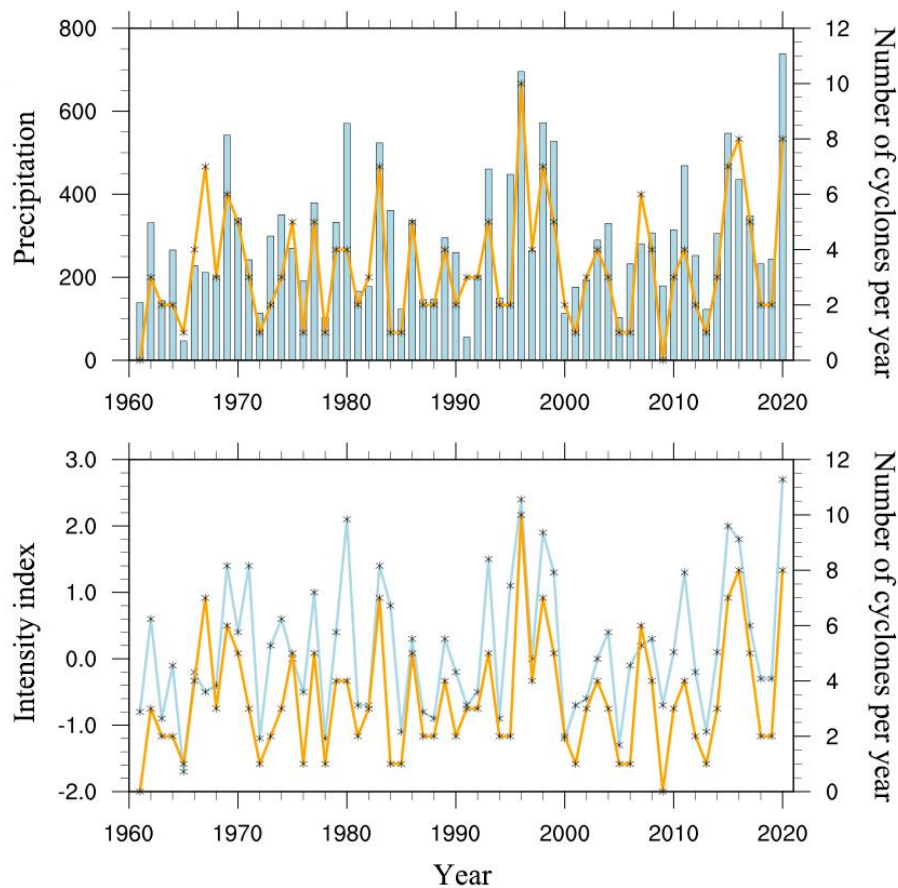
262 The Jianghuai cyclones are mainly active in the middle and lower reaches of the
263 Yangtze River (Huang et al., 2019; Li et al., 2002). Under the influence of the
264 strengthening westward extension of the WPSH during the Meiyu period, the Jianghuai

265 cyclones are restricted from entering the sea to some extent (Qin et al., 2015; Wu et al.,
266 2020). They form rainstorms and gales in the middle and lower reaches of the Yangtze
267 River and the coastal areas. A large part of the precipitation in the Meiyu period comes
268 from cyclone precipitation (Zhang et al., 2018). The intensity of Meiyu is usually
269 expressed by the Meiyu intensity index. The intensity of precipitation is affected not
270 only by precipitation but also by the number of precipitation days in the Meiyu period.
271 Both jointly determine the intensity of Meiyu in that year. The Meiyu intensity index is
272 defined as:

$$273 \quad M = \frac{L}{L_0} + \frac{0.5(R/L)}{R_0/L_0} + \frac{R}{R_0} - 2.5$$

274 M is the Meiyu intensity index. L is the length of the Meiyu in a given year (unit:
275 day) and L_0 means the average length of the Meiyu over the years (units: day). R is the
276 total precipitation of Jianghuai River basin during Meiyu in a given year, and R_0 is the
277 average total precipitation of Jianghuai River basin during Meiyu over the years. Where
278 M between -0.375 and 0.375, China Meteorological Administration defines this year as
279 the normal. Where M between 0.375 and 1.25, this year is defined as a little strong.
280 Where M greater than or equal to 1.25, this year is defined as strong. Where M between
281 -1.25 and -0.375, this year is defined as a little weak. Where M less than or equal to -
282 1.25, this year is defined as weak (GB/T 33671-2017).

283 The time-series plots of the number of cyclones related to precipitation and the
284 intensity index during the Meiyu period from 1961 to 2020 are given in Figure 6a and
285 6b. We found that the number of cyclones has a positive correlation coefficient of 0.769
286 with precipitation in the Meiyu period passing the 99% confidence interval according
287 to the T test. The number of cyclones was also positively correlated with the Meiyu
288 intensity index, with a correlation index of 0.760 passing the 99% confidence interval
289 according to the T test. The frequency of Jianghuai cyclone activity in years with a
290 strong Meiyu index is high; the frequency of Jianghuai cyclone activity in years with a
291 weak Meiyu index is low.



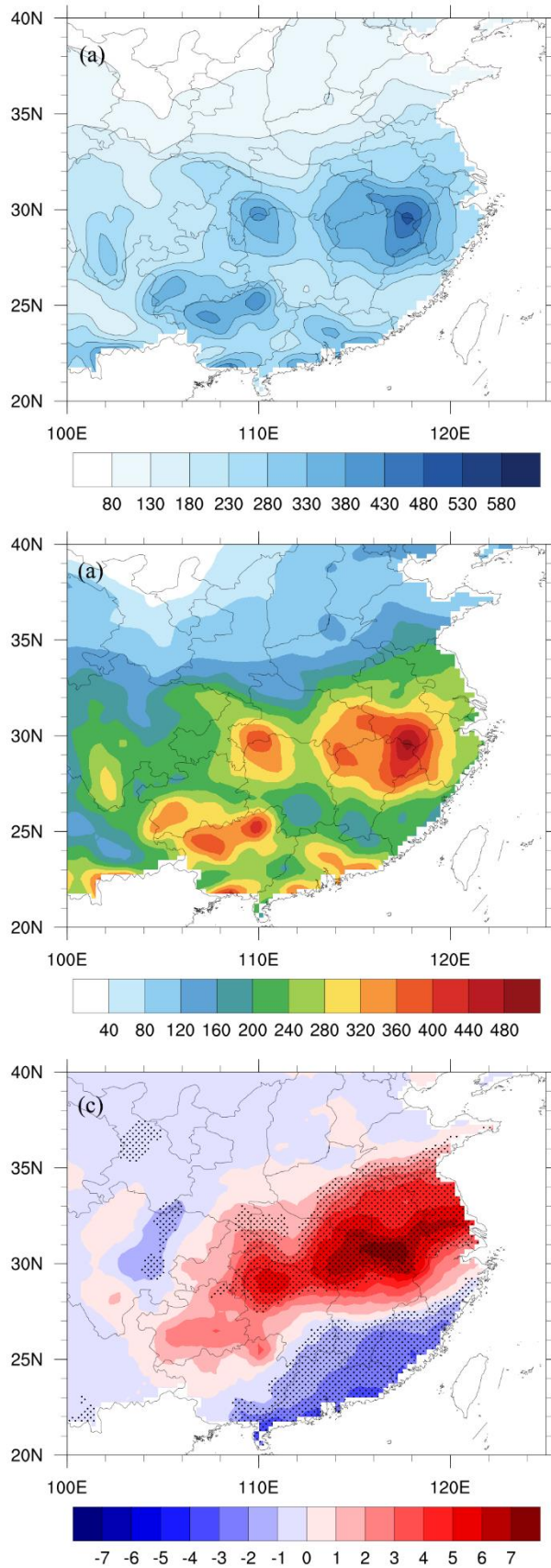
292 Fig 7. (a) Changes in precipitation (blue bar chart) (unit: mm/day) and the number of
 293 cyclones (orange line); (b) intensity index (blue line) and the number of cyclones
 294 (orange line) in the Meiyu period from 1961 to 2020.

295 Figure 8a shows the spatial distribution of annual average precipitation during the
 296 Meiyu period from 1961 to 2020. The areas with large precipitation values in the middle
 297 and lower reaches of the Yangtze River are mainly located in the Dabie Mountains of
 298 Anhui Province, the northern part of Jiangxi Province, the eastern part of Hubei
 299 Province and the western part of Hubei Province. The maximum annual average
 300 precipitation during the Meiyu period in southern Anhui can even exceed 480 mm. The
 301 occurrence of large precipitation areas during the Meiyu period is closely related to the
 302 topography of the region (Wu et al., 2023).

303 If precipitation and Jianghuai cyclone activity existed on the same day during the
 304 Meiyu period, we defined that day as a Jianghuai cyclone precipitation day. The

305 remaining days in the Meiyu period were treated as non-Jianghuai cyclone precipitation
306 days. Figure 8b shows the spatial distribution of the proportion of cyclone precipitation
307 relative to total precipitation during the Meiyu period. As shown in the figure, the main
308 areas affected by cyclone precipitation are the middle and lower reaches of the Yangtze
309 River. The Huaihe River basin in northern Anhui Province is the most affected area.
310 The cyclone precipitation in the Huaihe River basin accounts for more than 47% of the
311 total precipitation during the Meiyu period, while the cyclone-influenced precipitation
312 in other areas accounts for more than 35% of the total precipitation. In general, the
313 degree of cyclone-influenced precipitation in the middle and lower reaches of the
314 Yangtze River shows an east–west band distribution and a gradual decrease from
315 coastal to inland areas. This indicates that the distribution of the large-value area and
316 the characteristics of the band distribution are related to the northeast and eastward
317 tracks of the Jianghuai cyclone. Its precipitation capacity gradually increases with the
318 development of cyclone movement.

319 Figure 8c shows the spatial distribution of the daily mean precipitation anomaly
320 of the Jianghuai cyclone. The shaded part indicates that the 95% confidence interval is
321 passed according to the T test. The anomaly is based on the whole Meiyu period from
322 1961 to 2020 (The exceptions mentioned below are also based on the whole Meiyu
323 period from 1961 to 2020). When the Jianghuai cyclone is active, the middle and
324 lower reaches of the Yangtze River to the east of 108°E show an abnormal increase in
325 precipitation. However, Fujian, Guangdong and other places show an abnormal
326 decrease. Among them, the maximum value of abnormally increased precipitation can
327 exceed 7 mm/day in areas such as southern Anhui, eastern Hubei and northern Jiangxi.
328 The large-value areas of precipitation anomalies are consistent with the large-value
329 areas of cyclone occurrence frequency sources. It is inferred that the spatial distribution
330 of precipitation anomalies has a connection with the distribution of cyclone genesis
331 locations. This phenomenon of increasing and decreasing precipitation anomalies is
332 bounded by approximately 27°N and distributed north–south in the form of dipoles.



333 Fig 8. (a) Annual mean precipitation during the Meiyu period from 1961 to 2020 (units:

334 mm/year); (b) proportion of Jianghuai cyclone precipitation relative to total
335 precipitation during the Meiyu period (units: %); (c) daily mean precipitation anomaly
336 of the Jianghuai cyclone during the Meiyu period (units: mm/day) (shadow indicates
337 passing the 95% confidence interval according to the T test).

338 Figure 9 shows the evolution of composite geopotential height and horizontal wind
339 anomalies for three different levels of Jianghuai cyclones from day -4 to +2 during the
340 Meiyu period. Composite geopotential height anomalies are significant at the 95%
341 confidence level based on a T test. Vectors are plotted if wind anomalies are significant
342 at the 95% confidence level based on a T test in at least one direction.

343 Day 0 is the day on which the cyclone first appears in the specified area. Most
344 areas of the lower and middle troposphere (700 hPa, 850 hPa) in the middle and lower
345 Yangtze River on day 0 are covered by significant negative geopotential height
346 anomalies with peak magnitudes greater than -11 gpm. There is a significant positive
347 geopotential height anomaly with a peak magnitude of over 13 gpm on the southeast
348 side of the negative geopotential height anomaly. These anomalies form meridional
349 dipole structures in the middle and lower troposphere geopotential height field. The
350 southwest wind anomaly is significant in the middle and lower reaches of the Yangtze
351 River. The south of Anhui Province and the north of Jiangxi Province are between the
352 positive geopotential height anomaly and negative geopotential height anomaly. The
353 existence of these anomalies indicates the enhancement of southwest rapids and the
354 strengthening of the WPSH. The negative geopotential height anomalies at 500 hPa
355 height on day 0 are mainly in Mongolia, Shanxi and other places. Strong southwest
356 wind anomalies exist between the positive and negative geopotential height anomalies.
357 The negative geopotential height anomalies in the Mongolian region exceed -7 gpm.

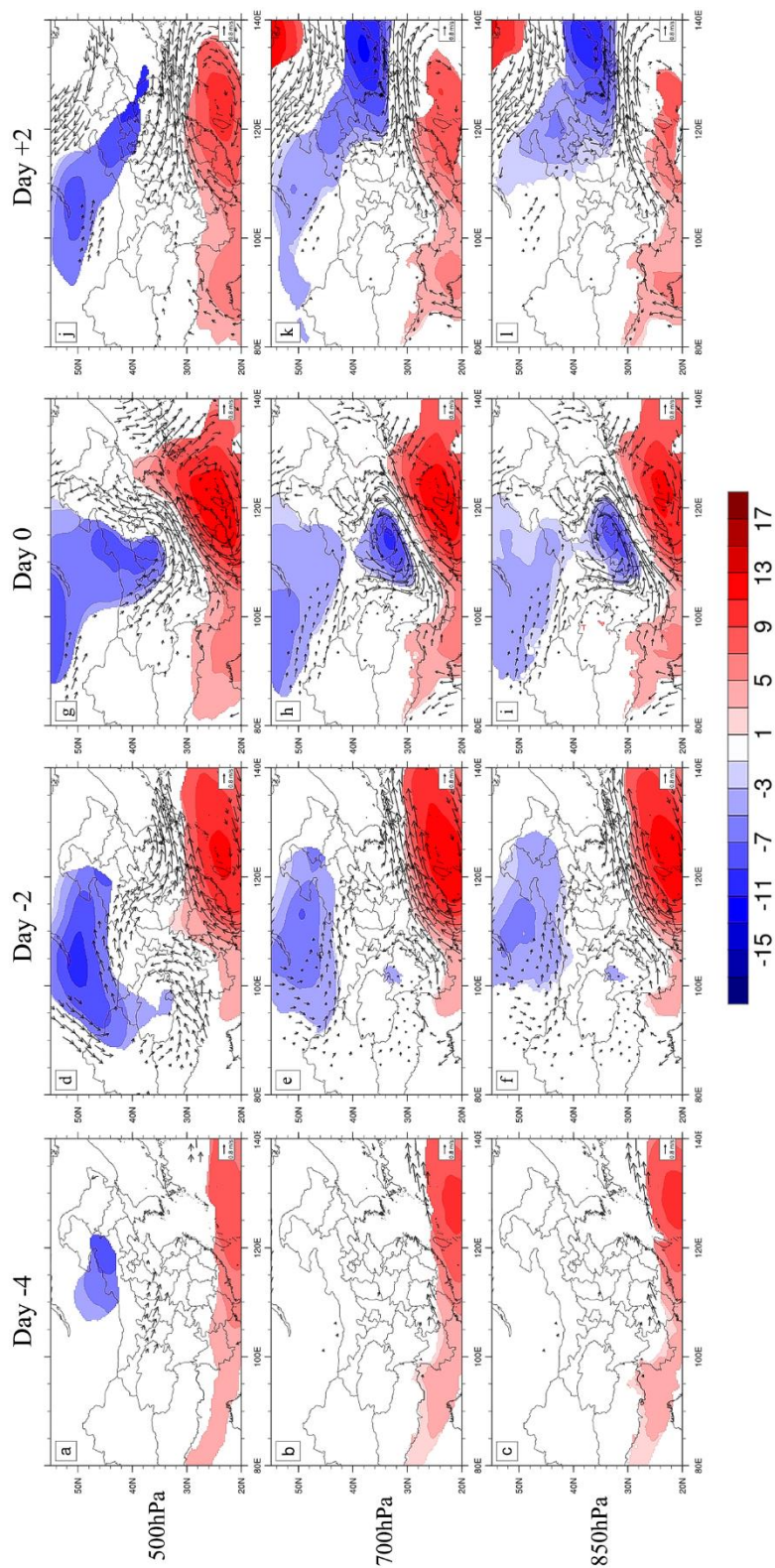
358 The negative geopotential height anomalies on all three isobaric surfaces can be
359 traced back to Mongolia, Inner Mongolia and part of Northeast China on day -2.
360 Negative geopotential height anomalies at 500 hPa can be traced to day -4. On day -4,
361 significant southwestern wind anomalies exist in southwestern Hunan at 700 hPa and

362 850 hPa. Significant northwest wind anomalies exist in the Yellow River basin of China
363 at 500 hPa. By day -2, the negative geopotential height anomalies in Mongolia, Inner
364 Mongolia and some northeastern areas are enhanced for all three isobars. The positive
365 geopotential height anomalies of the WPSH are enhanced and extend northward to the
366 southern part of the middle and lower reaches of the Yangtze River. There are
367 significant southwest wind anomalies at the three isobaric surfaces in the south of the
368 middle and lower reaches of the Yangtze River, while there are significant northwest
369 wind anomalies at 500 hPa in the north of Anhui Province and Jiangsu Province. The
370 negative geopotential height anomalies on the three isobaric surfaces move eastward
371 with the formation and development of Jianghuai cyclones. On day +2, the lower
372 reaches of the Yangtze River are mainly affected by the combined action of anomalous
373 southwest winds and northwest winds. The positive geopotential height anomaly of the
374 WPSH is weakened.

375 Therefore, the abnormal precipitation caused by the Jianghuai cyclone mainly
376 comes from the abnormal southwest winds and the strengthening of the WPSH. The
377 enhanced southwest jet provides sufficient warm and moist air for the formation of
378 cyclones and promotes the eastward migration of cyclones after formation. Liu et al.
379 (2020) and Zhao et al. (2021) studied the causes of the super strong Meiyu year in 2020,
380 mentioned that the WPSH is unusually strong and westward accompanied by an
381 abnormal increase in precipitation. Liu et al. (2020) found that the enhanced southwest
382 jet stream is conducive to the development of vertical movement in the middle and low
383 levels, which provides the necessary dynamic conditions for the formation of sustained
384 precipitation during the Meiyu in 2020.

385 Cold air activity is one of the important factors for the formation of heavy
386 precipitation, which can promote the convergence and uplift of low level necessary for
387 heavy precipitation (Liu et al., 2020). The enhanced negative geopotential anomaly
388 over Mongolia provides cold and dry air brought by the westerly jet for cyclone
389 development. The increasing frequency of cyclones over the Yangtze River and Huaihe
390 River leads to the abnormal increase in precipitation in the middle and lower reaches of

391 the Yangtze River during the Meiyu period. However, due to the strengthening of the
 392 WPSH, the southern part of China is controlled by the abnormal positive geopotential
 393 height, and the precipitation decreases. Zhao et al. (2021) also found that when the
 394 WPSH enhanced, there was a decrease in precipitation in South China.



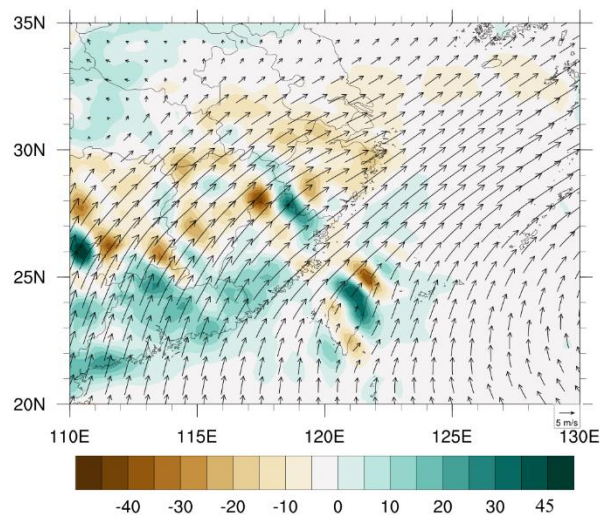
395 Fig 9. Evolution of composite geopotential height anomalies (shading; units: gpm) and
396 horizontal wind anomalies (units: m/s) on the 850 hPa, 700 hPa, and 500 hPa isobaric
397 surfaces for day -4 (a-c), day -2 (d-f), day 0 (g-i) and day +2 (j-l) for the 202 selected
398 Jianghuai cyclones. Shading indicates that composite geopotential height anomalies are
399 significant at the 95% confidence level based on a T test. Vectors are plotted if wind
400 anomalies are significant at the 95% confidence level based on a T test in at least one
401 direction.

402 Figure 10 shows the climatic distribution of water vapor flux and water vapor flux
403 divergence at a pressure level of 850 hPa during the Meiyu period. The water vapor
404 involved in the precipitation process of the Jianghuai cyclone during the Meiyu period
405 mainly comes from the water vapor brought by the southwest jet of the summer
406 monsoon in the low-latitude area. During Jianghuai cyclone development, the middle
407 and lower reaches of the Yangtze River are mostly in the water vapor convergence area,
408 which is conducive to the generation of precipitation (Chen et al., 2020).

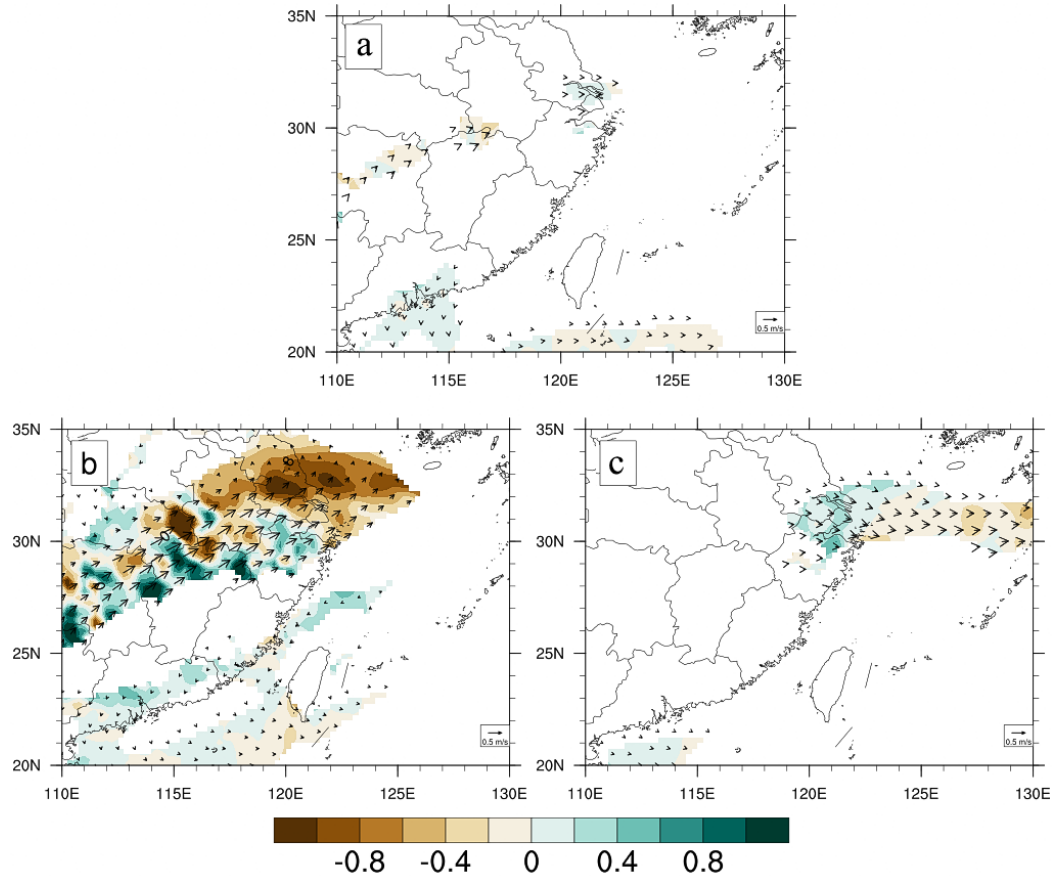
409 Figure 11 shows the distribution of water vapor flux anomalies and water vapor
410 flux divergence anomalies at the pressure level of 850 hPa during the Jianghuai cyclone
411 from day -2 to day +2. The color field and wind vector arrows in the figure both passed
412 the 95% significance according to the T test. On day -2, a significant water vapor
413 convergence anomaly and water vapor transport in the southwest direction appear in
414 southern Anhui Province. The anomalies of water vapor flux and water vapor flux
415 dispersion are mainly concentrated on day 0. There is significant anomalous water
416 vapor convergence up to $-1 \text{ g} \cdot \text{cm}^{-2} \cdot \text{hPa}^{-1}$ in eastern Hubei Province, Anhui Province and
417 Jiangsu Province on day 0. Anomalous water vapor dispersion exists in the southern
418 part of the middle and lower reaches of the Yangtze River and some areas in southern
419 China. On day +2, with the development of the cyclone's eastward movement, only the
420 southern part of Jiangsu Province and the northern part of Zhejiang Province have
421 abnormal water vapor flux in the eastward direction. The precipitation in the area begins
422 to gradually weaken at this time.

423 From day -2 to day 0, the abnormal water vapor flux and water vapor flux
424 divergence configuration make the warm and wet air in the low-latitude area transport
425 to the middle and lower reaches of the Yangtze River. The abnormal water vapor flux
426 has a negative value, water vapor convergence occurs, local water vapor volume
427 increases, and finally, the precipitation in the region increases. Liu et al. (2020) studied
428 the strong rainfall in 2020, they found that there was an enhanced water vapor transport,
429 and the repeated occurrence of convergence movement. Both of them caused the
430 precipitation time to increase in the Jianghuai River basin.

431 In contrast, the anomaly of water vapor flux in southern Guangdong and other
432 regions is divergent. This leads to a decrease in local water vapor volume and
433 precipitation in this region. These results indicate that the variations in water vapor flux
434 and divergence related to cyclones are mainly from warm and wet air transported from
435 low latitudes to the middle and lower reaches of the Yangtze River. Therefore, there is
436 a positive correlation between cyclone activity and precipitation in the middle and
437 lower reaches of the Yangtze River.



438 Fig 10. Distribution of 850 hPa daily mean water vapor flux (unit: $\text{g}\cdot\text{cm}^{-2}\cdot\text{hPa}^{-1}$) and
439 water vapor flux divergence (unit: $10^{-8}\text{ g}\cdot\text{cm}^{-2}\cdot\text{hPa}^{-1}\cdot\text{s}^{-1}$) of cyclones over the Yangtze
440 and Huaihe rivers during 1961-2020 (color diagram shows water vapor flux divergence,
441 and vector diagram shows water vapor flux).



442 Fig 11. Distribution of the 850 hPa daily mean water vapor flux anomaly (unit: $\text{g}\cdot\text{cm}^{-2}\cdot\text{hPa}^{-1}$) and water vapor flux divergence anomaly (unit: $10^{-8} \text{g}\cdot\text{cm}^{-2}\cdot\text{hPa}^{-1}\cdot\text{s}^{-1}$) of
 443 cyclones over the Yangtze and Huaihe rivers during 1961-2020 (color diagram shows
 444 water vapor flux divergence, and vector diagram shows water vapor flux). The colored
 445 region passed the 95% confidence interval according to a T test. If the vapor flux
 446 anomaly is significant at the 95% confidence level for the T test in at least one direction
 447 (zonal or meridian), the vector is plotted.
 448

449 4. Summary and discussion

450 Based on ERA5 reanalysis of sea level pressure data and using the relative
 451 vorticity method to identify and track cyclones, we have examined the impacts of the
 452 climatological characteristics of Jianghuai cyclones. The linkages between cyclone
 453 activity and precipitation in the middle and lower reaches of the Yangtze River during
 454 the Meiyu period are also analyzed.

455 During the Meiyu period, Jianghuai cyclones are mainly generated at the junction
456 of western Hubei and Chongqing Municipality, eastern Hubei Province, northern
457 Jiangxi Province, central and southern Anhui Province, and Jiangsu and Zhejiang
458 provinces. These cyclones develop and move to the sea in the east or northeast direction.
459 There is a positive correlation between the maximum intensity and maximum radius of
460 Jianghuai cyclones. The higher the cyclone intensity is, the larger the radius will be. Its
461 occurrence frequency not only has the characteristics of multicycle variation but also
462 has obvious interdecadal variation, which has a good correspondence with the periodic
463 and interdecadal variation in precipitation in the Meiyu period.

464 There is a positive correlation between the frequency of cyclone activity and
465 precipitation in the Meiyu period. The frequency of Jianghuai cyclone activity is high
466 in the years with strong Meiyu rainfall and low in the years with weak Meiyu rainfall.
467 The percentage of precipitation affected by Jianghuai cyclone activity in the middle and
468 lower reaches of the Yangtze River can reach up to 47%. The spatial distribution is in
469 the shape of an east–west belt, and the degree of influence gradually decreases from the
470 coast to the interior. When the Jianghuai cyclone is active, the precipitation increases
471 abnormally in the middle and lower reaches of the Yangtze River east of 108°E.
472 Precipitation decreases abnormally in Fujian Province and Guangdong Province. The
473 spatial distribution of precipitation anomalies is related to the genesis locations of
474 cyclone frequency, and the positive and negative anomalies are distributed north–south
475 in the form of dipoles based on the latitude line at approximately 27°N as the boundary.

476 The geopotential height anomaly field and the horizontal wind vector anomaly
477 field of the Jianghuai cyclones during the Meiyu period are synthesized and analyzed.
478 There is an enhanced positive geopotential height anomaly of the WPSH during cyclone
479 activity. The negative geopotential altitude anomaly of Mongolia and the abnormal
480 southwest jet are enhanced. All of these factors lead to an increase in precipitation in
481 the middle and lower reaches of the Yangtze River. The abnormal leading signal of the
482 negative geopotential height in Mongolia can be traced to day -2 of the cyclone activity,
483 and the signal can be traced to day -4 at 500 hPa. From day -2 to day 0 of cyclone

484 activity, the abnormal distribution of water vapor flux and water vapor flux divergence
485 cause the warm and wet air at the low latitudes to be transported to the middle and lower
486 reaches of the Yangtze River. They promote the generation and development of
487 cyclones and increase precipitation in the middle and lower reaches of the Yangtze
488 River.

489 We explored the cyclone characteristics and study emphasizes the link between
490 cyclone activity and Yangtze River precipitation. Spatially, abnormal precipitation
491 patterns are identified, tracing the evolution of geopotential height anomalies and water
492 vapor flux. But the specific mechanism by which the southwest jet affects cyclones
493 during the Meiyu period is not clear enough. Zhang et al. (2018) suggest that the
494 strengthening of the Southwest jet will lead to the development of α mesoscale low-
495 pressure disturbance near the Meiyu Front and the occurrence of extreme precipitation.
496 Liu et al. (2020) found that the strengthening of the southwest jet made the southerly
497 meridional strong gradient zone on the north side of the meridional wind maximum
498 center move northward in the low-level dynamic conditions of the rainstorm process
499 during Meiyu. How the Southwest jet stream influences the development of physical
500 factors to promote the formation of Jianghuai cyclones remains to be considered and
501 analyzed. Zhao et al. (2010) found that the causes of Jianghuai cyclones with different
502 intensities were different through a case study. Therefore, we think it is also necessary
503 to consider the difference in the influence of different intensities of Jianghuai cyclones
504 on precipitation. These problems need further analysis and research.

505 **Competing interests**

506 The contact author has declared that none of the authors has any competing interests.

507 **References**

- 508 Bao, Y, Y.: Similarities and Differences of Monsoon Circulations between 2016 and
509 1998 Meiyu Periods in Middle and Lower Reaches of the Yangtze River and
510 Comparison of Their Physical Mechanisms. Chinese Journal of Atmospheric
511 Sciences., 45, 994–1006, 2021. DOI: [10.3878/j.issn.1006-9895.2101.20174](https://doi.org/10.3878/j.issn.1006-9895.2101.20174)
- 512 Cai, Y, X., He, H., Lu, H., Zhu, L, Y., and Lu, Q, Q.: Synoptic and climatic
513 characteristics of persistent rainstorm in Guangxi in June 2020. Journal of
514 Meteorological Research and Application., 4, 113-117, 2021.
515 DOI:[10.19849/j.cnki.CN45-1356/P.2021.1.20](https://doi.org/10.19849/j.cnki.CN45-1356/P.2021.1.20).
- 516 Chen, L, J., Zhao, J, H., Gu, W., Liang, P., Zhi, R., Peng, J, B., Zhao, S, Y., Gao, H., Li,
517 X. and Zhang, P, Q.: Advances of Research and Application on Major Rainy Seasons
518 in China. Journal Of Applied Meteorological Science., 30, 385-400, 2019.
519 DOI: [10.11898/1001-7313.20190401](https://doi.org/10.11898/1001-7313.20190401)
- 520 Chen, T., Zhang, F, H., Yu, C., Ma, J., Zhang, X, D., Shen, X, L., Zhang, F. and Luo,
521 Q.: Synoptic analysis of extreme Meiyu precipitation over Yangtze River Basin during
522 June-July. Meteor Mon., 46, 1415-1426, 2020.
523 DOI: [10.7519/j.issn.1000-0526.2020.11.003](https://doi.org/10.7519/j.issn.1000-0526.2020.11.003)
- 524 Ding, Y, H.: Summer monsoon rainfalls in China. J Meteor Soc Jpn.,70, 373-396, 1992.
525 DOI: https://doi.org/10.2151/jmsj1965.70.1B_373
- 526 Ding, Y, H.: Seasonal march of the east-Asian summer monsoon. Chang C P. East Asian
527 Monsoon. Hackensack: World Scientific., 64, 2004.
528 DOI: https://doi.org/10.1142/9789812701411_0001
- 529 Ding, Y, H., Liu, J, J., Sun, Y., Liu, Y, J., He, J, H., Song, Y, F.: A Study of the Synoptic-
530 Climatology of the Meiyu System in East Asia. China J Atmos Sci., 31, 1082-1101,
531 2007. DOI: <https://d.wanfangdata.com.cn/periodical/daqikx200706006>
- 532 GB/T 33671-2017, Meiyu monitoring indices.
533 DOI:http://fj.cma.gov.cn/zfxxgk/zwgk/flfgbz/dfbz/202209/t20220921_5098384.htm
534 1
- 535 He, L, F., Chen, T., Zhou, Q, L. and Li, Z, C.: The Meso-β Scale Convective System of

536 a Heavy Rain Event on July 10, 2004 in Beijing. Journal Of Applied Meteorological
537 Science., 18, 655-665, 2007. DOI: [10.3969/j.issn.1001-7313.2007.05.010](https://doi.org/10.3969/j.issn.1001-7313.2007.05.010)

538 Hersbach, H., and Coauthors.: ERA5 hourly data on pressure levels from 1940 to
539 present. Copernicus Climate Change Service (C3S) Climate Data Store (CDS)., 2018.
540 DOI: [10.24381/cds.bd0915c6](https://doi.org/10.24381/cds.bd0915c6)

541 Hodges, K. I.: A general method for tracking analysis and its application to
542 meteorological data. Monthly Weather Review., 122, 2573-2586, 1994.
543 DOI:[https://doi.org/10.1175/1520-0493\(1994\)122<2573:AGMFTA>2.0.CO;2](https://doi.org/10.1175/1520-0493(1994)122<2573:AGMFTA>2.0.CO;2).

544 Hodges, K, I.: Feature tracking on the unit sphere. Monthly Weather Review., 123,
545 3458-3465, 1995.
546 DOI:[https://doi.org/10.1175/1520-0493\(1995\)123<3458:FTOTUS>2.0.CO;2](https://doi.org/10.1175/1520-0493(1995)123<3458:FTOTUS>2.0.CO;2).

547 Huang, W, Y., Sun, Y., Lu, C, H., Yao, L, N. and Dong, Q.: Statical analysis of Jianghuai
548 cyclone causing Jianguo regional heavy rain in summer nearly 40 years. Meteor Mon.,
549 45, 843-853, 2019. DOI: [10.7519/j.issn.1000-0526.2019.06.010](https://doi.org/10.7519/j.issn.1000-0526.2019.06.010)

550 Jiang, L, Z., Fu, S, M., Sun, J, H.: New method for detecting extratropical cyclones: the
551 eight-section slope detecting method. Atmospheric and Oceanic Science Letters, 13,
552 436-442, 2020.
553 DOI:[10.1080/16742834.2020.1754124](https://doi.org/10.1080/16742834.2020.1754124).

554 Jiangsu Provincial Weather Bureau: Jiangsu Province Weather Forecast Techniacal
555 Manual. Beijing: China Meteorological Press., 22-33, 2017.

556 Li, B., Yu, W, P., Lu, Y. and Lu, D, C.: The numerical simulating study of the mesoscale
557 characteristics on development of Jianghuai cyclones. Science meteorologic., 22, 72-
558 80, 2002. DOI: [10.3969/j.issn.1009-0827.2002.01.009](https://doi.org/10.3969/j.issn.1009-0827.2002.01.009).

559 Liang, P., Chen, L, J., Ding, Y, H., He, J, H. and Zhou, B.: Relationship between long-
560 term variability of Meiyu over the Yangtze River and ocean and Meiyu's
561 predictability study. Acta Meteorologica Sinica., 76, 379-393, 2018.
562 DOI:[10.11676/qxxb2018.009](https://doi.org/10.11676/qxxb2018.009).

563 Liu, Y, Y., Ding, Y, H.: Characteristics and possible causes for extreme Meiyu in 2020.
564 Meteor Mon.,46, 1393-1404, 2020. DOI: [10.7519/j.issn.1000-0526.2020.11.001](https://doi.org/10.7519/j.issn.1000-0526.2020.11.001)

565 Lu, C, H.: A Modified Algorithm for Identifying and Tracking Extratropical Cyclones.
566 Advances in atmospheric sciences., 34, 909-924, 2017.DOI: [10.1007/s00376-017-](https://doi.org/10.1007/s00376-017-6231-2)
567 [6231-2](https://doi.org/10.1007/s00376-017-6231-2)

568 Pascal, J, Mailier., David, B, Stephenson., Christopher, A, T, Ferro.: Serial Clustering
569 of Extratropical Cyclones. Monthly weather review, 134, 2224-2240, 2006.

570 Ninomiya, K., Murakami, T.: The early summer rainy season (Baiu) over Japan.
571 Monsoon Meteorology., New York: Oxford University Press, 93-121, 1987.

572 Oh, T, H., Kwon, W, T., Ryoo, S, B.: Review of the researches on Changma and future
573 observational study. Adv Atmos Sci, 14, 207-222, 1997.

574 Pang, Y., Wang, L, J. and Yu, B.: The relationship between 10-30d low frequency
575 oscillation and the rainfall over Changjiang-Huaihe River valley during Meiyu
576 period. Trans Atmos Sci., 36, 742-750, 2013.
577 DOI: [10.3969/j.issn.1674-7097.2013.06.011](https://doi.org/10.3969/j.issn.1674-7097.2013.06.011)

578 Qian, W, H., Lee, D, K.: Seasonal march of Asian summer monsoon. Int J Climatol.,
579 20, 1371-1386, 2000.
580 DOI: [10.1002/1097-0088\(200009\)20:11<1371::AID-JOC538>3.0.CO;2-V](https://doi.org/10.1002/1097-0088(200009)20:11<1371::AID-JOC538>3.0.CO;2-V)

581 Qin, T., Wei, L, X.: The statistic and variance of cyclones entering coastal waters of
582 china in 1979-2012. Acta Oceanologica Sinica., 2015.
583 DOI: [10.3969/j.issn.0253-4193.2015.01.005](https://doi.org/10.3969/j.issn.0253-4193.2015.01.005)

584 Saito, N.: Quasi-stationary waves in mid-latitudes and Baiu in Japan. J Meteor Soc, 63,
585 983-995, 1995.

586 Shen, Y., Sun, Y., Cai, N, H., Su, X. and Shi, D, W.: Analysis on the generation and
587 evolution of a Jianghuai Cyclone responsible for extreme precipitation event. Meteor
588 Mon.,45, 166-179, 2019. DOI: [10.7519/j.issn.1000-0526.2019.02.003](https://doi.org/10.7519/j.issn.1000-0526.2019.02.003)

589 Simmonds, I., Keay, K.: Mean Southern Hemisphere extratropical cyclone behavior in
590 the 40-year NCEP-NCAR reanalysis. J Climate., 13, 873-885, 2000.
591 DOI: [10.1175/1520-0442\(2000\)013<0873:MSHECB>2.0.CO;2](https://doi.org/10.1175/1520-0442(2000)013<0873:MSHECB>2.0.CO;2)

592 Simmonds, I., Murray, R, J.: Southern extratropical cyclone behavior in ECMWF
593 analyses during the FROST special observing periods. *Weather& Fore-casting.*, 14,
594 878-891, 1999.
595 DOI:[10.1175/1520-0434\(1999\)014<0878:SECBIE>2.0.CO;2](https://doi.org/10.1175/1520-0434(1999)014<0878:SECBIE>2.0.CO;2)

596 Su, X., Kang, Z, M., Zhuang, X, R. and Chen, S, J.: Uncertainty analysis of heavy rain
597 belt forecast during the 2020 Meiyu period. *Meteor Mon.*, 47, 1336-1346, 2021. DOI:
598 [10.7519/j.issn.1000-0526.2021.11.003](https://doi.org/10.7519/j.issn.1000-0526.2021.11.003).

599 Tao, S, Y., Ding, Y, H. and Zhou, X, P.: Study on heavy rain and severe convective
600 weather. *Chinese Journal of Atmospheric Sciences.*1979.

601 Wang, J, H., Niu, D., Ren, S, Y., Miao, C, S. and Song, P.: Comparative Study On
602 Development Of Different Deep Jianghuai Rivers Cyclones Entering the Sea and the
603 Influence of Environmental Factors. *Journal Of Tropical Meteorology.*, 31, 744-756,
604 2016. DOI: [10.16032/j.issn.1004-4965.2015.06.003](https://doi.org/10.16032/j.issn.1004-4965.2015.06.003).

605 Wang, Y, L., Wang, L, J.: Characteristics of southern cyclone activity and its influence
606 on precipitation in Yangtze River Basin. *Yangtze River.*, 43, 34-36,68, 2012. DOI:
607 [10.3969/j.issn.1001-4179.2012.09.009](https://doi.org/10.3969/j.issn.1001-4179.2012.09.009).

608 Wang, Y, L., Guan, Z, Y., Jin, D, C. and Ke, D.: Climatic characteristics and interannual
609 variations of cyclones over Changjiang-Huaihe River basin during late spring and
610 early summer from 1980 to 2012. *Trans Atmos Sci.*, 38, 354-361, 2015.
611 DOI: [10.13878/j.cnki.dqkxxb.20130413010](https://doi.org/10.13878/j.cnki.dqkxxb.20130413010)

612 Wang, L, J., Huang, Q, L., Li, Y. and Han, S, R.: Relationship between spatial
613 inhomogeneous distribution of Meiyu rainfall over the Yangtze-Huaihe River Valley
614 and previous SST. *Trans Atmos Sci*, 37, 313-322, 2014. DOI: [10.3969/j.issn.1674-7097.2014.03.008](https://doi.org/10.3969/j.issn.1674-7097.2014.03.008)

615

616 Wei, J, S., Liu, J, Y., Sun, Y. and Xu, Y, C.: Climate characteristics of Jiang-Huai
617 cyclone. *J Meteor Sci*, 33, 196-201, 2013. DOI: [10.3969/2012jms.0112](https://doi.org/10.3969/2012jms.0112)

618 Wernli, H., Schwierz, C.: Surface cyclone in the ERA-40 dataset (1958-2001). Part I:
619 Novel identification method and global climatology. *J Atmos Sci.*, 63, 2486-2507,
620 2006.

621 Wu, J, F., Xu, X, F., Zhao, W, R., Qing, Q. and Zou, L.: Characteristics of Persistent
622 Heavy Rainfall and Water Vapor Transport in Western Sichuan Plateau.
623 Meteorological science and technology., 48, 704-716, 2020.
624 DOI:[10.19517/j.1671-6345.20190301](https://doi.org/10.19517/j.1671-6345.20190301).

625 Wu, Q., Chen, S, J., Bai, Y., Xia, L. and Wang, C, J.: Diagnostic analysis and numerical
626 simulation of a heavy rainstorm associated with the Jianghuai cyclone. Journal of the
627 Meteorological Sciences., 41, 86-98, 2021. DOI: [10.12306/2020jms.0029](https://doi.org/10.12306/2020jms.0029).

628 Wu, Q., Liu, T., Zhang, B., Zhang, Y. and Wang, Y.: A Comparative Analysis of the
629 Heavy Rainstorm Processes of Two Jianghuai Cyclones. Anhui Agri, Sci, Bull., 26,
630 161-171, 2020. DOI: [10.3969/j.issn.1007-7731.2020.09.058](https://doi.org/10.3969/j.issn.1007-7731.2020.09.058)

631 Wu, Q., Feng, J, W., Wang, Y., Chen, Y. and Zhang, L, T.: Spatial and temporal
632 distribution of cyclones over the Jianghuai River during 1979-2018. Meteorology of
633 Shanxi., 06, 15-22, 2021. DOI: [10.3969/j.issn.1006-4354.2020.06.003](https://doi.org/10.3969/j.issn.1006-4354.2020.06.003)

634 Wu, T., Xu, G, Y., Li, S, J. and Wei, F.: Characteristics and Causes of a Mixed-Type
635 Convective Weather During the Formation and Development of a Jianghuai Cyclone
636 in Spring. Advances in Meteorological Science and Technology., 48, 704-716, 2023.
637 DOI:[10.19517/j.1671-6345.20190301](https://doi.org/10.19517/j.1671-6345.20190301).

638 Xu, J., Zhou, C, Y. and Gao, T, C.: Analysis about Development Mechanism of
639 Jianghuai Cyclone in Meiyu Front and Its Relationship with Rainstorm. Bulletin Of
640 Science and Technology., 29, 24-29,86, 2013.
641 DOI: [10.3969/j.issn.1001-7119.2013.05.006](https://doi.org/10.3969/j.issn.1001-7119.2013.05.006).

642 Xu, J, M.: Satellite Imagery Characteristics for Extratropical Cyclones and Meiyu Font.
643 Advances in Meteorological Science and Technology., 11, 14-26, 2021. DOI:
644 [10.3969/j.issn.2095-1973.2021.03.003](https://doi.org/10.3969/j.issn.2095-1973.2021.03.003)

645 Xu, Y, C., Wei, J, S. and Zhu, W, J.: A numerical simulation and marine sensitive
646 experiments of Jiang-Huai cyclone. J Meteor Sic., 31, 726-731, 2011.
647 DOI: [10.3969/j.issn.1009-0827.2011.06.008](https://doi.org/10.3969/j.issn.1009-0827.2011.06.008)

648 Yan, J, R., Wang, W, J., Zhang, H. and Shi, D, W.: Analysis of two rainstorm and gale
649 processes of Jianghuai cyclone in Jiangsu Province in 2019. Journal of

650 Meteorological Research and Application., 42, 83-88, 2021.
651 DOI: [10.19849/j.cnki.CN45-1356/P.2021.2.16](https://doi.org/10.19849/j.cnki.CN45-1356/P.2021.2.16)

652 Yang, Y, M., Gu, W, L., Zhao, R, L. and Liu, J.: The statical analysis of vortex during
653 Meiyu season in the lower reaches of the Yangtze. Quarterly Journal of Applied
654 Meteorology., 21, 11-18, 2010. DOI: [10.3969/j.issn.1001-7313.2010.01.002](https://doi.org/10.3969/j.issn.1001-7313.2010.01.002)

655 Zhao, B, K., Wu, G, X. and Yao, X, P.: A diagnostic analysis of potential vorticity
656 associated with development of a strong cyclone during the Meiyu period of 2003.
657 Chinese Journal of Atmospheric Sciences., 32, 1241-1255, 2008.
658 Doi: [10.3878/j.issn.1006-9895.2008.06.02](https://doi.org/10.3878/j.issn.1006-9895.2008.06.02).

659 Zhao, B, k., Wan, R, J. and Lu, X, Q.: A Contrastive Analysis on the Causes of Strong
660 and Weak Cyclones over Yangtze-Huaihe River Valleys during the Meiyu Period in
661 Summer of 2003. Plateau Meteorology., 29, 309-320, 2010.

662 Zhao, J, H., Chen, L, J. and Wang, D, Q.: Characteristics and causes analysis of
663 abnormal Meiyu in China in 2016. Chinese Journal of Atmospheric Sciences., 42,
664 1055-1066, 2018. DOI: [10.3878/j.issn.1006-9895.1708.17170](https://doi.org/10.3878/j.issn.1006-9895.1708.17170)

665 Zhao, J, H., Zhang, H., Zuo, J, Q., Xiong, K, G. and Chen, L, J.: What Drives the Super
666 Strong Precipitation over the Yangtze–Huaihe River Basin in the Meiyu Period of
667 2020. Chinese Journal of Atmospheric Sciences., 45, 1433–1450, 2021.
668 Doi: [10.3878/j.issn.1006-9895.2104.2101](https://doi.org/10.3878/j.issn.1006-9895.2104.2101).

669 Zhang, X, L., Tao, S, Y. and Zhang, S, L.: Three Types of Heavy Rainstorms Associated
670 with the Meiyu Front. Chinese Journal of Atmospheric Sciences, 28., 187-205, 2004.
671 doi: [10.3878/j.issn.1006-9895.2004.02.03](https://doi.org/10.3878/j.issn.1006-9895.2004.02.03)

672 Zhang, X, L., Tao, S, Y. and Zhang, Q, Y.: An Analysis on Development of MESO- β
673 Convective System along Meiyu Front Associated with Flood in Wuhan in 20-21
674 July 1998, Journal of Applied Meteorological Science., 13, 385-397, 2002. DOI:
675 [10.3969/j.issn.1001-7313.2002.04.001](https://doi.org/10.3969/j.issn.1001-7313.2002.04.001).

676 Zhang, X, H., Luo, J., Chen, X., Jin, L, L. and Qiu, X, M.: Formation and development
677 mechanism of one cyclone over Changjiang-Huaihe River basin and diagnostic
678 analysis of rainstorm. Meteor Mon., 42, 716-723, 2016.

679 DOI: [10.7519/j.issn.1000-0526.2016.06.007](https://doi.org/10.7519/j.issn.1000-0526.2016.06.007)

680 Zhang, J, G., Wang, J., Wu, T., Zhou, J, L., Zhong, M., Wang, S, S., Huang, X, Y., Li,
681 S, J., Han, F, R. and Wang, X, C.: Weather system types of extreme precipitation in
682 the middle reaches of the Yangtze River. *Torrential Rain and Disasters.*, 37, 14-23,
683 2018.

684 Doi: [10.3969/j.issn.1004-9045.2018.01.003](https://doi.org/10.3969/j.issn.1004-9045.2018.01.003)

685 Zhang, Y, X., Ding, Y, H. and Li, Q, P.: Cyclogenesis Frequency Changes of
686 Extratropical Cyclones in the Northern Hemisphere and East Asia Revealed by
687 ERA40 Reanalysis Data. *Meteor Mon.*, 38, 646-656, 2012.

688 Zhou, J, L., Zhang, J, G., Wu, T., Xu, G, Y., Liu, X, W., Wang, J. and Han, F, R.:
689 Characteristics of the mesoscale weather system producing extreme rainstorm in
690 boundary layer during the Meiyu front over the middle reaches of Yangtze River.
691 *Meteor Mon.*, 48, 1007-1019, 2022. DOI: [10.7519/j.issn.1000-0526.2022.052801](https://doi.org/10.7519/j.issn.1000-0526.2022.052801)

692 Zhong, Q, M., Ma, J., Wang, L.: Biweekly oscillation of the Meiyu-season precipitation
693 in 2016 and 2020 over the Yangtze Huaihe River basin: A comparative analysis. *Acta*
694 *Meteorologic Sinica.*, 8, 235-25, 2023. DOI: [10.11676/qxxb2023.20220075](https://doi.org/10.11676/qxxb2023.20220075)

695 Zhou, X, M., Zheng, Y, G.: Analysis of Environmental Conditions and Tornado Storm
696 Features of Two Tornadoes in Jiangsu during the Meiyu Period in 2020. *Advances in*
697 *Meteorological Science and Technology.*, 10, 34-42, 2020.

698 DOI: [10.3969/j.issn.2095-1973.2020.06.008](https://doi.org/10.3969/j.issn.2095-1973.2020.06.008).

699 Zhou, Y. , Xia, L.: Statistical Research on Climatic Characteristics of Jianghuai
700 Cyclones. *Meteorological and Environmental Sciences.*, 40, 79-85, 2017.

701 DOI: [10.16765/j.cnki.1673-7148.2017.03.013](https://doi.org/10.16765/j.cnki.1673-7148.2017.03.013)

702 Zhu, M., Lu, H, C. and Yu, Z, H.: Study of Positive Feedback Mechanism for Meso- α
703 Scale Cyclone Growing on Meiyu Front. *Chinese Journal of Atmospheric Sciences.*,
704 22, 763-770, 1998. Doi: [10.3878/j.issn.1006-9895.1998.05.11](https://doi.org/10.3878/j.issn.1006-9895.1998.05.11)